

6-11-2004

Optimization of Thermal Interface Materials for Electronics Cooling Applications

Vishal Singhal

Thomas Siegmund

S V. Garimella

Purdue Univ, sureshg@purdue.edu

Follow this and additional works at: <http://docs.lib.purdue.edu/coolingpubs>

Singhal, Vishal; Siegmund, Thomas; and Garimella, S V, "Optimization of Thermal Interface Materials for Electronics Cooling Applications" (2004). *CTRC Research Publications*. Paper 32.

<http://docs.lib.purdue.edu/coolingpubs/32>

This document has been made available through Purdue e-Pubs, a service of the Purdue University Libraries. Please contact epubs@purdue.edu for additional information.

Optimization of Thermal Interface Materials for Electronics Cooling Applications

Vishal Singhal, Thomas Siegmund, and Suresh V. Garimella

Abstract—Thermal interface materials (TIMs) are used in electronics cooling applications to decrease the thermal contact resistance between surfaces in contact. A methodology to determine the optimal volume fraction of filler particles in TIMs for minimizing the thermal contact resistance is presented. The method uses finite element analysis to solve the coupled thermo-mechanical problem. It is shown that there exists an optimal filler volume fraction which depends not only on the distribution of the filler particles in a TIM but also on the thickness of the TIM layer, the contact pressure and the shape and the size of the filler particles. A contact resistance alleviation factor is defined to quantify the effect of these parameters on the contact conductance with the use of TIMs. For the filler and matrix materials considered—platelet-shaped boron nitride filler particles in a silicone matrix—the maximum observed enhancement in contact conductance with the use of TIMs was by a factor of as much as 9.

Index Terms—Contact resistance reduction, electronics cooling, finite element analysis, interface materials, thermal contact conductance.

NOMENCLATURE

E	Elastic modulus (N/m ²).
f	Contact resistance alleviation factor (dimensionless).
h	Thickness of filler particles (m).
k	Thermal conductivity (W/mK).
l	Thickness of unit cell (m).
p	Contact pressure (N/m ²).
q''	Distributed heat flux (W/m ²).
r	Width (m).
R	Resistance (Km ² /W).
T	Temperature (K).
u	Displacement (m).
V	Volume fraction (dimensionless).
x	x-coordinate (m).
y	y-coordinate (m).

Greek Symbols

ε	Average strain (dimensionless).
σ	rms surface roughness (m).
ν	Poisson's ratio (dimensionless).
$\tan \theta$	Average slope of the asperities (dimensionless).
ΔT	Mean temperature difference (K).

Subscripts and Superscripts

1	Material/surface/particle 1.
---	------------------------------

2	Material/surface/particle 2.
b	Bulk.
c	Contact.
eq	Equivalent value.
f	Filler.
NOTIM	Without thermal interface material.
o	Undeformed.
TIM	With/of thermal interface material.
u	Unit cell.
x	x-direction.
y	y-direction.

I. INTRODUCTION

ANY ENGINEERING surface is rough on a microscopic level, due to the presence of microscopic asperities. When two such rough surfaces come in contact, the actual contact occurs only at a few discrete spots, usually at the high points of the two surfaces [Fig. 1(a)]. Heat flowing from one body into the other is constricted to flow through the actual contact spots, because the thermal conductivity of the solid contact spots is much higher than that of the surrounding gap which is filled with air in most engineering applications [1].

Thermal interface materials (TIMs) are often inserted between the surfaces of a contact pair to reduce the thermal contact resistance. Although they typically have lower thermal conductivity than the substrate, they are highly compliant and hence under the application of relatively small contact pressures, deform to conform to the geometry of the adjacent rough surfaces. A part of the low thermal conductivity gas present [Fig. 1(b)] is thus replaced by a higher conductivity material. This leads to a decrease in the constriction of the heat flow lines, and hence, an increase in the contact conductance.

The two most desirable properties of a TIM are high thermal conductivity and high compliance. Since relatively few homogeneous materials possess both these properties, TIMs are typically composite materials with metallic or ceramic fillers in a polymeric matrix. Typically used fillers such as alumina (Al₂O₃) or boron nitride (BN) are characterized by relatively high thermal conductivity and low compliance. Most matrix materials, e.g., silicone, have low thermal conductivity but high compliance. In view of practical applications, optimal volume fractions and geometric distributions of filler and matrix materials are sought at which the contact conductance assumes a maximum value. The optimal filler volume fraction is expected to depend on a series of factors, including the relative thermal and mechanical properties of the matrix and filler, the filler shape, its distribution and orientation. Furthermore, the size of the filler particles relative to the thickness of the

Manuscript received May 1, 2003; revised August 12, 2003. This work was recommended for publication by Associate Editor K. C. Toh upon evaluation of the reviewers' comments.

The authors are with the School of Mechanical Engineering, Purdue University, West Lafayette, IN 47907-2088 USA (e-mail: sureshg@ecn.purdue.edu).

Digital Object Identifier 10.1109/TCAPT.2004.828587

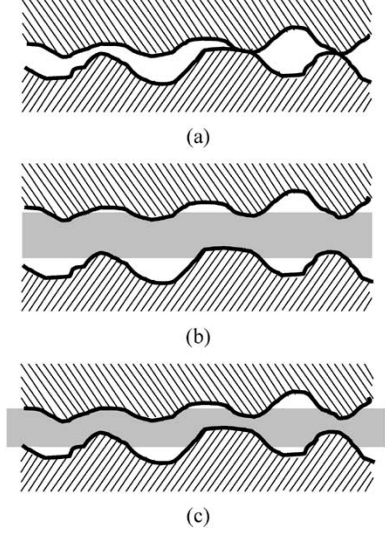


Fig. 1. Schematic illustration of contact between two rough surfaces (a) without a TIM, (b) with a TIM at low contact pressure, and (c) with a TIM at high contact pressure.

TIM layer will also affect the optimal filler volume fraction, as will the boundary resistance between filler and matrix. The objective of this work is to find the volume fraction and the geometric distribution of filler particles for which the contact conductance of a ‘rough surface-TIM-rough surface’ system takes the maximum value. The effect of the various parameters identified above on the optimal filler volume fraction and contact conductance are documented.

Most of the past work on TIMs has been targeted toward experimental determination of the effects of parameters such as contact pressure, filler volume fraction, TIM layer thickness and nonplanarity of the contacting surfaces on the thermal conductivity of TIMs [2]–[5]. Devpura *et al.* [6], [7] used percolation theory to model TIMs, and investigated the influence of changes in parameters such as the ratio of conductivity of the filler particles to that of the matrix material, filler volume fraction, TIM layer thickness and shape and size of the filler particles on the thermal conductivity. However, their work is a study of the effect of these parameters on the thermal conductivity of the TIM itself and does not determine the effect of TIMs in decreasing the contact resistance. Other numerical models [4], [8] have also not considered the variation of contact resistance and are limited to a study of the variation of thermal conductivity. These models do not address the net effect of TIMs in decreasing thermal contact resistance, as they do not account for the effect of the deformation of the TIMs. Recently analytical models based on the surface chemistry [9] and the wettability of the TIMs [10] have been presented to predict their thermal contact resistance.

II. CONTACT CONDUCTANCE ANALYSIS

For elastic contact between two rough substrates, the thermal contact resistance is given by [11]

$$R_c = \frac{1}{1.55} \left(\frac{\sigma}{k_{eq} \tan \theta} \right) \left[\frac{E_{eq} \tan \theta}{\sqrt{2p}} \right]^{0.94}. \quad (1)$$

Here, E_{eq} is the equivalent elastic modulus, k_{eq} the equivalent thermal conductivity of the two contacting materials, p the contact pressure, σ the rms surface roughness, and $\tan \theta$ the average slope of the asperities on the two contacting substrate surfaces. For machined surfaces the asperity slope can be calculated using $\tan \theta = 0.125\sigma^{0.402}$ for surface roughnesses ranging from 0.27 to 12 μm [12].

Using the expressions for equivalent elastic modulus, $1/E_{eq} = (1 - \nu_1^2)/E_1 + (1 - \nu_2^2)/E_2$, and equivalent thermal conductivity, $2/k_{eq} = 1/k_1 + 1/k_2$, the contact resistance for contact between two similar rough metallic surfaces with equal surface roughness and slope of asperities, ($R_{c,NOTIM}$) can be calculated as

$$R_{c,NOTIM} = \frac{1}{1.55} \left(\frac{\sigma}{\tan \theta} \right) \left[\frac{E_1 \tan \theta}{2\sqrt{2p}(1 - \nu_1^2)} \right]^{0.94} \left(\frac{1}{k_1} \right) \quad (2)$$

in which k_1 is the thermal conductivity, E_1 the elastic modulus, and ν_1 the Poisson’s ratio of the two bodies in contact.

If, however, a TIM layer is inserted between the two rough surfaces, the composite thermal resistance between the rough surfaces will consist of three components: Two due to the contact of the TIM layer with the rough surfaces on either side ($R_{c,TIM,1}$ and $R_{c,TIM,2}$) and a third arising from the bulk resistance of the TIM layer ($R_{b,TIM}$). The latter quantity $R_{b,TIM}$ is calculated as the ratio of the thickness of the TIM layer to the thermal conductivity of the TIM. Assuming that the two contact pairs on both sides of the TIM are similar (in particular, with identical material properties and surface roughnesses), and that the stiffness of the TIM is much smaller than that of the two bodies in contact, $R_{c,TIM,1}$ and $R_{c,TIM,2}$, are given by

$$R_{c,TIM,1} = R_{c,TIM,2} = \frac{1}{1.55} \left(\frac{\sigma}{\tan \theta} \right) \times \left[\frac{E_{TIM} \tan \theta}{\sqrt{2p}(1 - \nu_{TIM}^2)} \right]^{0.94} \frac{1}{2} \left(\frac{1}{k_1} + \frac{1}{k_{TIM}} \right) \quad (3)$$

in which E_{TIM} is the elastic modulus of the TIM in the axial y -direction (Fig. 2), ν_{TIM} the Poisson’s ratio for compression in the axial direction and expansion in the lateral x -direction, and k_{TIM} the through-thickness thermal conductivity of the TIM. The values of E_{TIM} , ν_{TIM} , and k_{TIM} used in the above equation are obtained from the finite element model described in the next section. Various effects, such as the increase in microhardness of the TIM due to the presence of filler particles close to surface and the increase in k_{TIM} due to the increase in effective path length of the filler particles with increase in load, are accounted for in the finite element model.

A nondimensional contact resistance alleviation factor, f , can now be defined as the ratio of the composite thermal resistance at the contact between two rough metallic surfaces with a TIM to that for bare contact between the same surfaces

$$f = \frac{R_{c,TIM}}{R_{c,NOTIM}} = \frac{R_{c,TIM,1} + R_{b,TIM} + R_{c,TIM,2}}{R_{c,NOTIM}}. \quad (4)$$

For a TIM to be beneficial, f should take a value smaller than 1. The factor f can be expressed as the sum of two components, f_c and f_b , where f_c is the ratio of the sum of the two contact

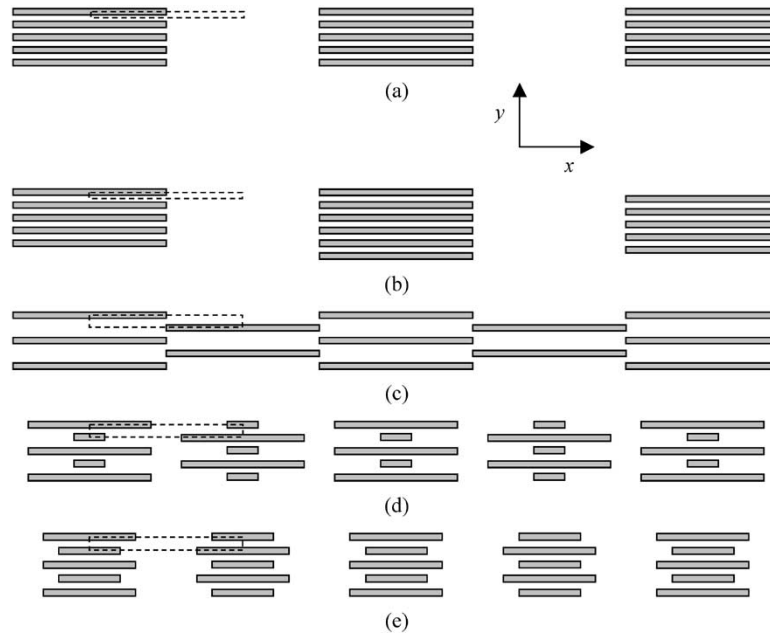


Fig. 2. Illustration of the different filler distributions studied: (a) inline, (b) staggered, (c) laterally staggered, (d) 20% bimodal, and (e) 40% bimodal distributions. The dotted rectangles show the unit cells used for the finite element analysis.

resistance components in $R_{c,TIM}$ to $R_{c,NOTIM}$, and f_b is the ratio of the bulk resistance of the TIM layer to $R_{c,NOTIM}$

$$f_c = \left[2 \frac{E_{TIM}}{E_1} \frac{(1 - \nu_1^2)}{(1 - \nu_{TIM}^2)} \right]^{0.94} \left(1 + \frac{k_1}{k_{TIM}} \right) \quad (5a)$$

and,

$$f_b = 1.55 \frac{\tan \theta}{\sigma} \left[\frac{2\sqrt{2}p(1 - \nu_1^2)}{E_1 \tan \theta} \right]^{0.94} k_1 R_{b,TIM}. \quad (5b)$$

It may be noted that f_c is only a function of the thermal and mechanical properties of the rough metallic surfaces and the TIM. It is independent of other factors such as surface topography (surface roughness and asperity slope) and TIM layer thickness. Although contact pressure p does not explicitly appear in (5a), f_c is in fact a weak function of contact pressure since f_c depends on the conductance in the TIM which changes with the amount of deformation applied. On the other hand, f_b depends both on the characteristics of the metallic surfaces, σ and θ , as well as the elastic and thermal properties of the substrate and the TIM layer. It is also dependent on the bulk resistance (and hence thickness) of the TIM layer, which changes with the deformation of the TIM. In addition, (5b) includes an explicit dependence of f_b on contact pressure.

In order to calculate $f = f_c + f_b$ for a TIM for its use between substrates with given surface roughness and material properties, the values of the elastic modulus (E_{TIM}), Poisson's ratio (ν_{TIM}) and thermal conductivity (k_{TIM}) of the TIM as well as the bulk resistance of the TIM layer ($R_{b,TIM}$) are needed. The value of f for a 'rough surface-TIM-rough surface' combination depends on the deformation of the TIM layer through the variation of the properties of the TIM layer. Hence, to calculate f for a given contact pressure, the deformation of the TIM layer needs to be determined with the TIM properties expressed for the deformed TIM layer. Since there are no analytical models available

to solve this class of problems if microstructural geometry is to be accounted for, the finite element method was chosen for the present study, by which the problem can be solved via coupled thermomechanical analyzes.

III. MODEL DEVELOPMENT

A. Microstructure of TIMs

The finite element model together with a unit cell approach is used to analyze TIMs. As is common in commercial TIMs, it is assumed that platelet-shaped boron nitride (BN) filler particles are present (aspect ratio 25:1) in a silicone matrix [13].

Five different types of filler particle distributions were studied to determine the effects of filler arrangement and size distribution on TIM properties, including:

- 1) inline;
- 2) staggered;
- 3) laterally staggered;
- 4) 20% bimodal;
- 5) 40% bimodal distributions.

These five distributions are illustrated in Fig. 2. Filler particles in the inline distribution are aligned both horizontally and vertically, and are all of the same size. The staggered and laterally staggered distributions also have all particles of the same size but platelets are aligned in one direction only and staggered in the horizontal or the vertical direction, respectively. For the bimodal distributions, two different sizes of filler particles are considered [Fig. 2(d) and (e)], with filler particles of different sizes alternating as neighbors.

The unit cell models for the filler particle distributions considered are shown in Fig. 3(a)–(c). The inline and the staggered distributions are modeled using the unit cell of Fig. 3(a), while the laterally staggered and the bimodal distributions are modeled using the unit cells of Fig. 3(b) and (c), respectively. In the figures, $r_{u,0}$ is the undeformed width of the unit cells and $h/2$

TABLE I
MODELING DETAILS OF UNIT CELLS IN FIG. 3

Unit cell	Static deformation modeling	Thermal modeling	Element type for bulk filler and matrix	Boundary elements for interface between filler and matrix
Figure 3(a)	Axi-symmetry along $x = 0$	Axi-symmetric heat conduction	Axi-symmetric coupled temperature displacement elements (CAX4T)	Axi-symmetric coupled temperature displacement interface elements (INTER2AT)
Figures 3(b) – 3(c)	Plane strain	2-D heat conduction	Plane strain coupled temperature displacement elements (CPE4T)	2-D coupled temperature displacement interface elements (INTER2T)

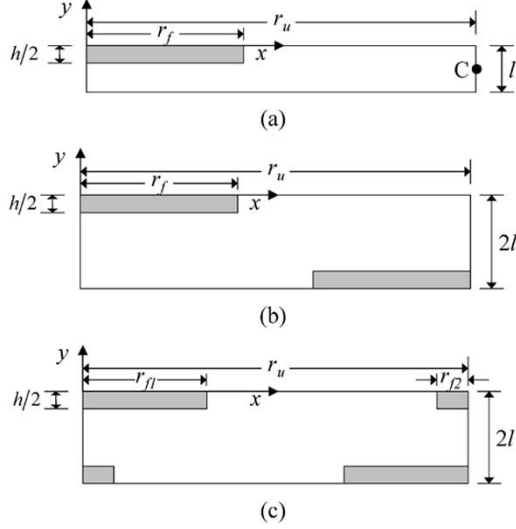


Fig. 3. Unit cell models of the TIM for filler volume fraction of 0.15 and (a) in-line and staggered, (b) laterally staggered, and (c) bimodal filler distributions.

is the thickness of the filler particles. The undeformed thickness of the unit cell is l_o for the unit cell in Fig. 3(a) and $2l_o$ for the unit cells in Fig. 3(b) and (c). In Fig. 3(a) and (b), r_f is the width of the filler particles. In Fig. 3(c) r_{f1} is the width of the larger filler particle and r_{f2} is the width of the smaller filler particle, such that $r_f = r_{f1} + r_{f2}$.

Fully coupled temperature-displacement analyzes are performed for the unit cell models by use of the commercially available finite element software package ABAQUS/Standard [14]. Model details for the different unit cells are given in Table I, and the boundary conditions and loads used in the analysis are summarized in Table II. The boundary conditions for the staggered distribution are extensions of the methods described in [15] and [16].

In order to calculate the values of f_c and f_b in (5), the values of E_{TIM} , k_{TIM} , ν_{TIM} , and $R_{b,TIM}$ are determined from the finite element analysis. The effective thermal conductivity k_{TIM} of a TIM layer is calculated as

$$k_{TIM} = q'' \frac{l}{\Delta T} \quad (6)$$

in which q'' is the distributed heat flux, l the deformed thickness of the unit cell and ΔT the calculated mean temperature difference between the top and bottom planes of the unit cell. Thus, the bulk resistance of the TIM layer is obtained from the numerical results as $R_{b,TIM} = l/k_{TIM}$. The quantity E_{TIM} is

obtained from the simulations as $E_{TIM} = p/|\varepsilon_{yy}|$, with ε_{yy} being the average strain in the unit cell in the y -direction given by, $\varepsilon_{yy} = (l/l_o) - 1$. For the unit cell in Fig. 3(a) ν_{TIM} is given by $\nu_{TIM} = -\varepsilon_{xx}/\varepsilon_{yy}$, and for the unit cells in Figs. 3(b) and (c) by $\nu_{TIM} = \varepsilon_{xx}/(\varepsilon_{xx} - \varepsilon_{yy})$.

The material properties of BN and silicone used in the analysis are listed in Table III. Both BN and silicone are assumed to behave as linear elastic materials. The effect of thermal boundary resistance between the filler particles and the matrix material is taken into account by use of interface elements that account for perfect mechanical load transfer and imperfect heat transfer between the filler and the matrix. The thermal boundary resistance between the filler particles and the matrix material was taken to be $0.03 \text{ Kcm}^2/\text{W}$ [13]. A representative surface roughness of $\sigma = 5 \mu\text{m}$, for contact between two rough metallic surfaces and between a metallic surface and a TIM, is used to calculate f_b .

IV. RESULTS

A. In-line and Staggered Distributions

The variation of k_{TIM} as a function of the volume fraction of filler, V_f , for the in-line distribution is shown in Fig. 4(a). Since the thermal conductivity of the filler particles is much higher than that of the matrix material, an increase in V_f leads to an overall increase in the thermal conductivity of the TIM, independent of pressure. An increase in the contact pressure also causes an increase in k_{TIM} . The filler particles are much stiffer than the matrix material, and hence deform less. This leads to an increase in the effective path length through the filler particles in the TIM as the contact pressure increases and the thickness of the TIM decreases, and results in an increase in k_{TIM} . The pressure dependence of k_{TIM} is more significant at higher values of V_f .

The corresponding dependence of f_c on V_f for different contact pressures is shown in Fig. 4(b). Results at low V_f are presented only for small pressures because of difficulties with numerical convergence when the pressures become comparable to the elastic modulus of the purely elastic silicone. A minimum value of f_c exists for a (nonextreme) volume fraction $V_f = 0.1$ for $p = 0.2 \text{ MPa}$. Since lower values of f_c imply higher contact conductance between the rough substrate surface and the TIM layer, the contact conductance exhibits a maximum for $V_f = 0.1$. It may be noted that Singhal *et al.* [17] found that for the case of *spherical* alumina filler particles in a silicone matrix, f_c is a minimum for $V_f = 0.5$, in contrast to the results for the

TABLE II
BOUNDARY CONDITIONS AND LOADS USED ON UNIT CELLS IN FIG. 3

Filler distribution (Unit cell) → Boundary Conditions ↓	Inline (3a)	Laterally staggered (3b)	bimodal (3c)	Staggered (3a)
	$y = 0$	<ul style="list-style-type: none"> • Symmetry plane relative to the y-direction^a • $T _{y=0} = T_o$ 		
$x = 0$	<ul style="list-style-type: none"> • $u_x(x=0) = 0$^b 			<ul style="list-style-type: none"> • $u_x(x=0) = 0$^b
$x = r_u$	<ul style="list-style-type: none"> • Remains parallel to its original configuration and the y-axis 			<ul style="list-style-type: none"> • $u_y(y=y_1) = -u_y(y=-l-y_1)$^d • $T(y=y_1) - T(y=-l/2) = T(y=-l/2) - T(y=-l-y_1)$^d • $u_x(y=y_1) + u_x(y=-l-y_1) = 2u_x(y=-l/2)$^e
$y = -l$	<ul style="list-style-type: none"> • Remains parallel to its original configuration and the x-axis 			<ul style="list-style-type: none"> • Remains parallel to its original configuration and the x-axis
Load	<ul style="list-style-type: none"> • Uniform distributed compressive load and uniform distributed heat flux at the bottom plane 			<ul style="list-style-type: none"> • Equal uniform distributed compressive loads at the top and the bottom planes and a uniform distributed heat flux at the bottom plane

^a Nodes along $y = 0$ cannot move in the y -direction but are free to move in the x -direction, except for the point (0,0).

^b $u_x(x=0)$ represents the displacement of the plane $x = 0$ in the x -direction.

^c The top and the bottom planes have equal but opposite deformation in the y -direction.

^d The right plane has symmetric deformation and temperature difference in the y -direction with respect to the center point C (Figure 3a). Hence, the point $(r_u, -l/2)$ is constrained in the y -direction.

^e The total cross-sectional area of two adjacent unit cells is independent of their y -coordinate. This is a linear form of $(r_u + u_x(y=y_1))^2 + (r_u + u_x(y=-l-y_1))^2 = 2(r_u + u_x(y=-l/2))^2$.

TABLE III
MATERIAL PROPERTIES OF THE FILLER AND THE MATRIX MATERIAL
USED IN THE FINITE ELEMENT MODEL [13]

	Elastic Modulus	Poisson's Ratio	Thermal Conductivity
Boron Nitride	675.0 GPa	0.05	20.0 W/(mK)
Silicone	1.0 MPa	0.40	0.2 W/(mK)

platelet-shaped particles in the present work. The results for the inline and the staggered distributions agreed to within 1% for the variation of both k_{TIM} and f_c , and only the results for the inline distribution are presented here.

The contact resistance alleviation factor f is plotted along with f_b and f_c in Fig. 4(c) for a contact pressure of 100 kPa and an undeformed TIM layer thickness of $l_o = 50 \mu\text{m}$. Clearly, f is a minimum for $V_f = 0.3$. Hence, the increase in composite contact conductance between the two metallic surfaces with the use of a TIM layer will be greatest for $V_f = 0.3$. It is also seen from the figure that f_b decreases monotonically with an increase in filler volume fraction. Results for the variation of f with V_f for a range of pressures (with $l_o = 50 \mu\text{m}$) are plotted in Fig. 4(d). Similar results for a variety of TIM thicknesses ($l_o = 50, 100,$ and $150 \mu\text{m}$) are shown in Fig. 4(e) at two different contact pressures of 100 and 400 kPa. Again, a nonmonotonic variation of f with V_f is observed in most of the cases, as addressed in the remainder of this section. In general, f increases with V_f at low contact pressures and small TIM thicknesses, while at high contact pressures, f decreases with V_f . Also, the optimal V_f (for f to be a minimum) varies with both the contact pressure and the

TIM layer thickness. For $l_o = 50 \mu\text{m}$, among the V_f values considered, the optimal V_f is 0.3 for contact pressures of 100 kPa and 0.8 for higher contact pressures [Fig. 4(d)].

The nonmonotonic variation of f with V_f for a given contact pressure p and undeformed length l_o may be explained as follows. As can be seen from Fig. 4(b), f_c increases monotonically with V_f (for $V_f \geq 0.1$). On the other hand, as the V_f in a TIM layer is increased for a given l_o and p , the effective thermal conductivity of the TIM layer k_{TIM} also increases and hence, $R_{b,\text{TIM}}$, the bulk resistance component of the composite resistance, decreases. This causes a decrease in f_b with increasing V_f . An increase in V_f thus causes two competing effects—an increase in f_c coupled with a decrease in f_b —such that $f = f_c + f_b$ is in general not a monotonic function of V_f . Also, the increase in f with l_o for a given contact pressure and filler volume fraction, observed in Fig. 4(e), is mainly due to the increase in f_b , since f_c for a TIM is independent of l_o and only a weak function of the contact pressure [Fig. 4(b)].

It is interesting to note that although the composite contact resistance of a “rough surface-TIM-rough surface” combination would be expected to decrease with increasing contact pressure, the value of f actually increases. This is because f is defined as the ratio of the composite contact resistance with the TIM to that without the TIM, and as the contact pressure increases, the contact resistance for bare-metal contact decreases at a faster rate than the composite contact resistance with the TIM. For the same reason, a lower value of f does not necessarily imply a lower composite contact resistance. At higher contact pres-

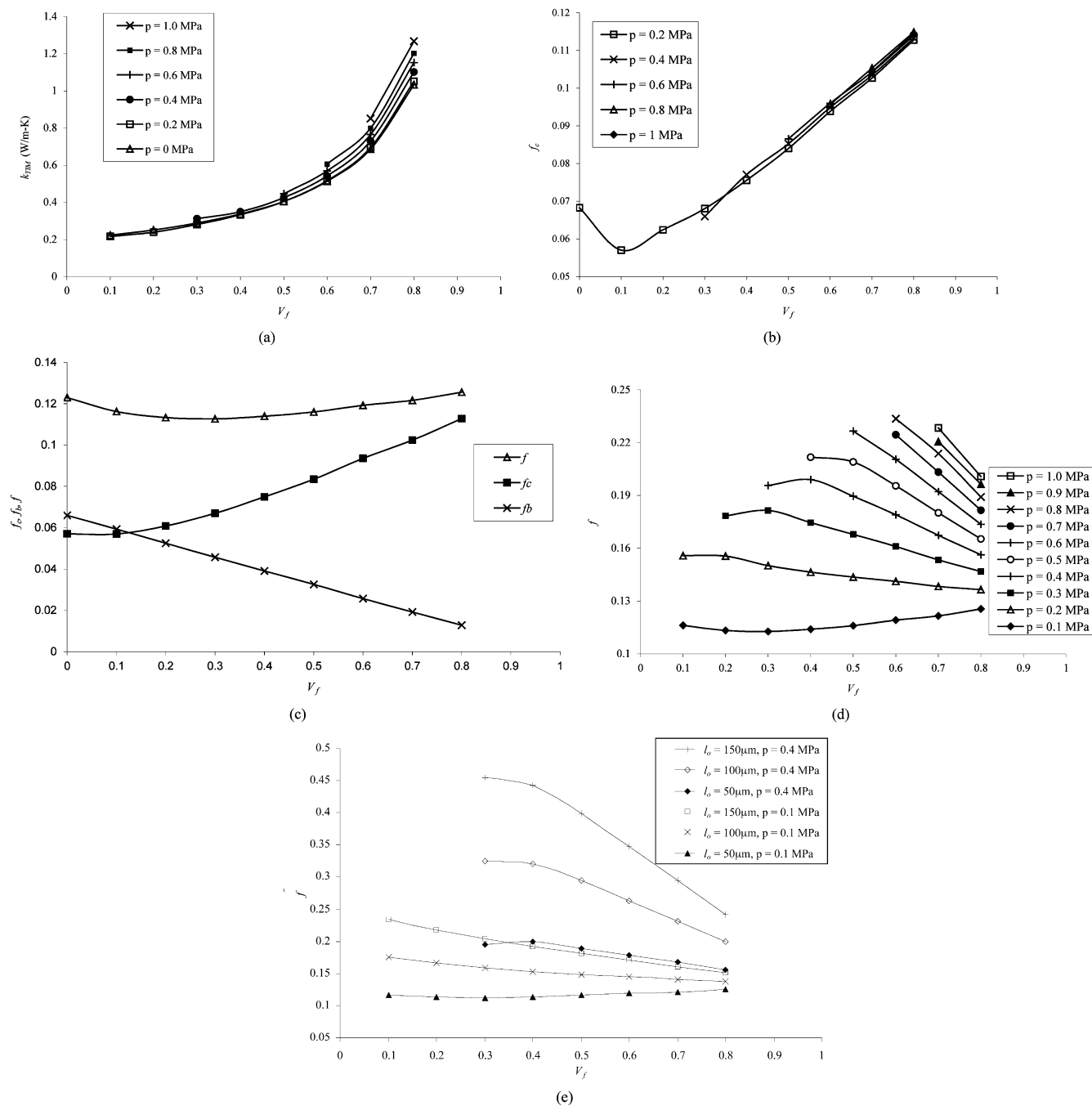


Fig. 4. Model prediction for inline distribution: (a) k_{TIM} , (b) f_c , (c) f_c , f_b , and f for $l_o = 50 \mu\text{m}$ and $p = 100 \text{ kPa}$, (d) f for $l_o = 50 \mu\text{m}$, and (e) f for different undeformed TIM thicknesses.

tures, although f_c is a monotonically increasing function of V_f , f generally decreases with increasing V_f , mainly at large filler volume fractions. This is because as the contact pressure increases, k_{TIM} increases and f_b decreases, with the effects being most pronounced at the larger filler volume fractions. Hence, in the variation of f with V_f , the effect of f_b dominates, leading to a decrease in f with increasing V_f at high contact pressures. This also leads to an increase in the optimal V_f with an increase in the contact pressure.

The optimal V_f values at a contact pressure of 100 kPa and for $l_o = 50, 100, \text{ and } 150 \mu\text{m}$ are 0.3, 0.8, and 0.8, respectively [Fig. 4(e)]. This increase in optimal filler volume frac-

tion with l_o is attributed to the increase in Rb_{TIM} and hence in f_b with increasing l_o , while f_c , which is independent of l_o , remains constant. Also, f_c is an increasing function and f_b a decreasing function of the filler volume fraction. Therefore, since an increase in the value of l_o causes an increase in f_b while f_c remains constant, f for a larger l_o will assume the minimum value for a larger filler volume fraction.

B. Laterally Staggered Distribution

For the laterally staggered distribution, the variation of k_{TIM} with V_f is qualitatively similar to that for the inline distribution, although the absolute values of k_{TIM} are higher by ap-

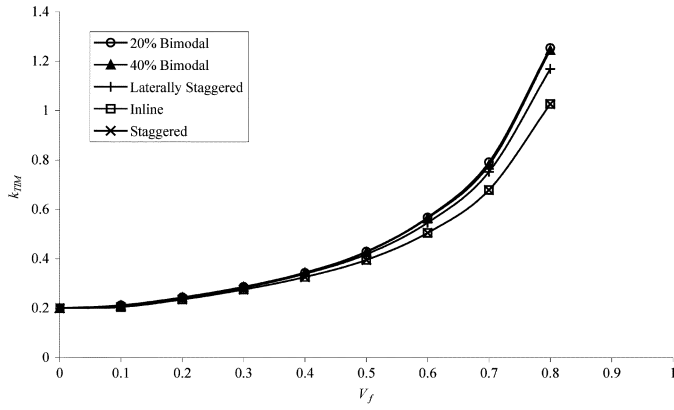


Fig. 5. Variation of k_{TIM} with filler volume fraction for $p = 0.1$ MPa under different distributions of filler particles.

proximately 10 to 20%. This is shown in Fig. 5 where k_{TIM} is plotted against V_f for different filler distributions. In addition, k_{TIM} increases more rapidly with an increase in V_f because in the laterally staggered distribution, the filler particles are more evenly distributed and hence cover more cross-sectional area for the same filler volume fraction than in the inline distribution [Fig. 2(c)].

The variation of f_c with V_f for this laterally staggered distribution is shown in Fig. 6 for a range of pressures from 100 kPa to 1 MPa. As for the inline distribution (Fig. 4(b)), f_c increases monotonically with V_f (except for $p = 0.4$ MPa) in the range of volume fractions considered. For a contact pressure of 100 kPa, as the V_f is increased from 0.1 to 0.8, E_{TIM} increases approximately by a factor of 9, while k_{TIM} increases only by a factor of 5. Since f_c increases with increasing E_{TIM} and decreases (less strongly) with increasing k_{TIM} , this results in a net increase in f_c with V_f .

The variation of f_c with contact pressure is different at different filler volume fractions. For small V_f , f_c increases with increasing contact pressure, whereas for large V_f , f_c decreases, resulting in a crossover in the behavior at $V_f \approx 0.5$. This effect mainly results from a stronger dependence of k_{TIM} on contact pressure at the larger filler volume fractions. For $V_f = 0.1$, an increase in contact pressure by 100 kPa causes k_{TIM} to increase approximately by 0.5% whereas E_{TIM} increases by $\approx 2.5\%$. Hence, for small filler volume fractions, f_c increases with increasing contact pressure. On the other hand, for $V_f = 0.8$, a similar increase in contact pressure by 100 kPa causes k_{TIM} to increase by $\approx 2.5\%$ whereas E_{TIM} still increases by $\approx 2.5\%$. Hence, f_c decreases with increasing contact pressure for large filler volume fractions. Such a trend of larger increases in k_{TIM} (with increasing contact pressure) for higher volume fractions was also observed for the inline distribution [Fig. 4(a)]. A curious aspect of Fig. 6 is that as V_f increases from 0.2 to 0.3, there is a much smaller increase in f_c than elsewhere in the curves. The reason for this behavior will be explained later in this section.

Qualitatively, the variation of f with V_f for the laterally staggered distribution is similar to the inline distribution [Fig. 4(c)]. However, quantitatively, at low contact pressures the absolute values of f are higher than those for the inline distribution for the same σ and l_o , while at high contact pressures f is lower

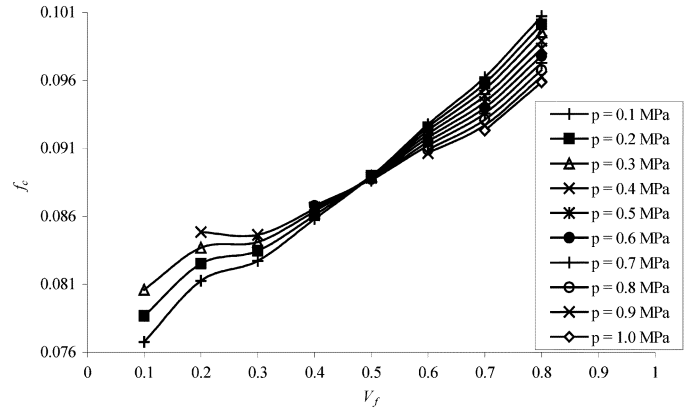


Fig. 6. Variation of f_c with filler volume fraction for the laterally staggered distribution.

than in the inline distribution. Hence, the inline distribution will result in greater alleviation in contact resistance as compared to the laterally staggered distribution at low contact pressures, while the laterally staggered distribution will lead to greater alleviation at high contact pressures. Again, as for the inline distribution, a nonextreme optimal filler volume fraction ($V_f = 0.5$) exists only for a contact pressure of 100 kPa with $l_o = 50 \mu\text{m}$. At all contact pressures > 100 kPa with $l_o = 50 \mu\text{m}$, and at all contact pressures considered for $l_o = 100$ and $150 \mu\text{m}$, f assumes the minimum value for $V_f = 0.8$. Also, as was the case for the inline distribution, the larger values of l_o lead to higher optimal V_f and *vice-versa*.

C. Bimodal Distributions

The variation of k_{TIM} with V_f and contact pressure in the case of the bimodal distributions follows similar trends as for the inline [Fig. 4(a)] and staggered distributions, but the absolute values of k_{TIM} are comparatively higher (by up to 30%), especially at the higher filler volume fractions (Fig. 5). The more favorable (i.e., more uniform) distribution of the filler particles through the cross section of the TIM layer leads to this behavior. For the bimodal distributions, the thermal boundary resistance between the filler particles and matrix material will have a greater impact on k_{TIM} because of the somewhat larger interface area between the filler and the matrix. However, since the typical thermal boundary resistance is very small ($0.03 \text{ Kcm}^2/\text{W}$ [13]), its deleterious effect is not very significant, and is swamped by the improvements in k_{TIM} due to the improved distribution of the filler particles. The variation of the contact resistance alleviation factor f with V_f for the bimodal distributions also follows the same trends as for the inline distribution. However, for the bimodal distributions, the optimal (minimum) value of f occurs at $V_f = 0.8$ for all contact pressures considered.

The variation of f_c with V_f at various contact pressures is shown in Fig. 7(a) and (b) for the 20% and the 40% bimodal distributions, respectively. The reversed trends observed for the variation of f_c with V_f at high and low contact pressures in the case of the laterally staggered distribution are also noticed for both the bimodal distributions. However, for the laterally staggered distribution, the increase in f_c with V_f was monotonic,

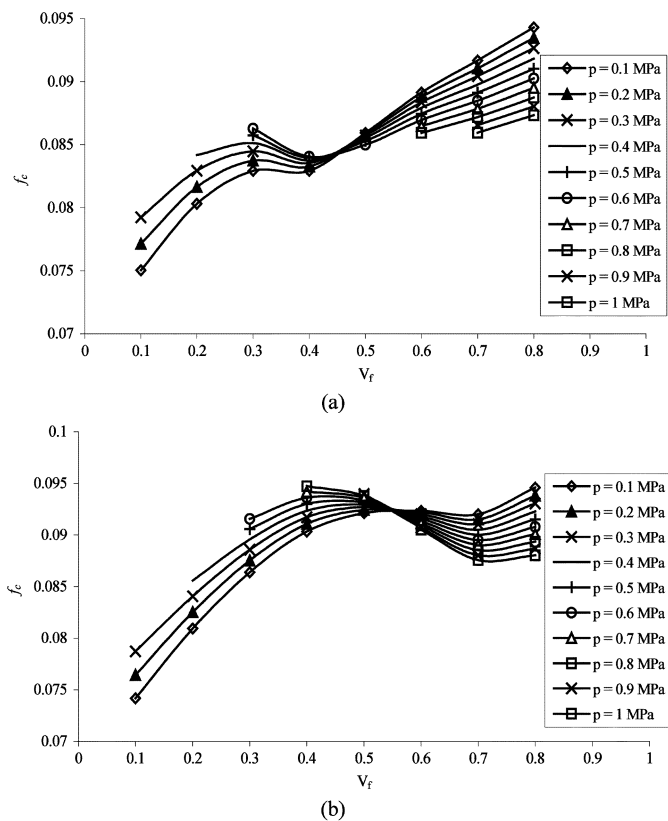


Fig. 7. Variation of f_c with filler volume fraction for (a) 20% and (b) 40% bimodal distributions.

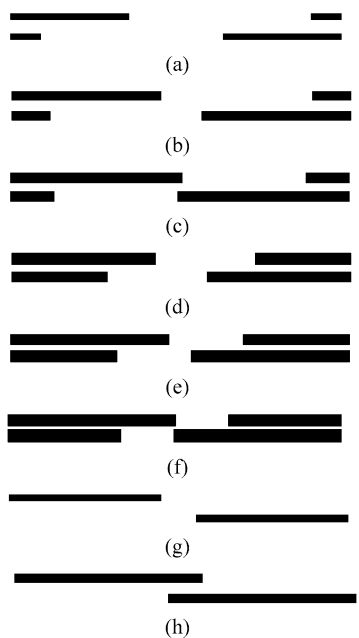


Fig. 8. Undeformed microstructure of TIMs for filler volume fractions of (a) 0.2, (b) 0.3, and (c) 0.4 for the 20% bimodal distribution, (d) 0.5, (e) 0.6, and (f) 0.7 for the 40% bimodal distribution, and (g) 0.2 and (h) 0.3 for the laterally staggered distribution.

whereas for both the bimodal distributions, the increase is non-monotonic. In fact, for the 40% bimodal distribution, there is an observable decrease in f_c with increasing V_f at the higher

contact pressures. This is explained by the higher thermal conductivity of the TIMs for large filler volume fractions, which causes a significant decrease in f_c . Another significant contributor to this effect is discussed in the following paragraph.

Considering the plot of variation of f_c with V_f for the 20% bimodal distribution at a contact pressure of 100 kPa [Fig. 7(a)], f_c is seen to increase monotonically with V_f at an approximately uniform rate except in the range of V_f from 0.3 to 0.4, where the increase is negligible. The undeformed microstructures of the TIM for the 20% bimodal distribution at $V_f = 0.2, 0.3$, and 0.4 are shown in Fig. 8(a)–(c), respectively. For $V_f = 0.2$ and 0.3, the filler particles do not overlap, leaving a part of the cross-sectional area in the TIM devoid of filler particles, whereas for $V_f = 0.4$, the particles do overlap. This causes the TIM for $V_f = 0.4$ to be much stiffer than that for $V_f = 0.3$. This negates the effect of any increase in k_{TIM} which occurs due to an increase in V_f . There is thus a negligible increase in f_c as V_f increases from 0.3 to 0.4 [Fig. 7(a)]. The same phenomenon is also observed for the 40% bimodal distribution [Fig. 7(b)], between $V_f = 0.6$ and 0.7. The undeformed microstructures of the TIM for the 40% bimodal distribution for the filler volume fractions of 0.5, 0.6, and 0.7 are shown in Fig. 8(d)–(f).

The same phenomenon of a muted increase in f_c due to a sudden increase in stiffness is noticed for the laterally staggered distribution as well. The undeformed microstructures of the TIM for $V_f = 0.2$ and 0.3 for the laterally staggered distribution are shown in Fig. 8(g) and (h), respectively. The filler particles are seen to overlap for $V_f = 0.3$, unlike the case for $V_f = 0.2$.

V. CONCLUSION

The variation of the contact resistance alleviation factor f with the volume fraction of platelet-shaped filler particles is studied for five different filler distributions to find the optimal filler volume fraction (V_f) and filler distribution in a thermal interface material (TIM) which would lead to a minimum value of contact resistance. The main conclusions from the present work are as follows.

- 1) A bimodal distribution of the filler particles leads to the highest effective thermal conductivity of the TIM.
- 2) An increase in the thickness of the TIM layer leads to an increase in the optimal V_f , and also a decrease in the effectiveness of the TIM.
- 3) Although the laterally staggered and the bimodal distributions lead to higher effective thermal conductivities (k_{TIM}) than the inline distribution, they lead to a smaller alleviation in the contact resistance because of their higher stiffness. This shows the importance of considering both the mechanical and thermal properties when selecting a TIM.
- 4) Contact pressure is also an important factor in selecting a TIM. The inline distribution leads to minimum contact resistance at low contact pressures, while the bimodal distributions lead to minimum contact resistance at relatively high contact pressures.

REFERENCES

- [1] C. V. Madhusudana, *Thermal Contact Conductance*. New York: Springer-Verlag, 1996.
- [2] M. de Sorigo, "A test device for measuring thermal impedance of heat transfer interface materials," *Power Conv. Intell. Motion*, vol. 11, pp. 59–62, 1985.
- [3] M. Early, S. Lee, and M. Pellilo, "Thermal performance of interface material in microelectronics packaging applications," in *Proc. IEPS'95 Conf.*, San Diego, CA, 1995, pp. 534–544.
- [4] R. F. Babus'Haq, P. W. O'Callaghan, and S. D. Probert, "Reducing the thermal resistance of a pressed contact by employing an interfacial filler," *Heat Transfer Eng.*, vol. 12, pp. 28–36, 1991.
- [5] N. F. Dean and A. L. Gettings, "Experimental testing of thermal interface materials on nonplanar surfaces," in *Proc. 14th IEEE Annual Semiconductor Thermal Measurement and Management Symp.*, 1998, pp. 88–94.
- [6] A. Devpura, P. E. Phelan, and R. S. Prasher, "Percolation theory applied to study the effect of shape and size of the filler particles in thermal interface materials," *Proc. ASME Heat Transfer Division*, vol. 4, pp. 365–371, 2000.
- [7] —, "Percolation theory applied to the analysis of thermal interface materials in flip-chip technology," *ITHERM*, vol. 1, pp. 21–28, 2000.
- [8] C. P. Chiu, G. L. Solbrekken, and T. M. Young, "Thermal modeling and experimental validation of thermal interface performance between non-flat surfaces," *ITHERM*, vol. 1, pp. 55–62, 2000.
- [9] P. Zhou and K. E. Goodson, "Modeling and measurement of pressure-dependent junction-spreader thermal resistance for integrated circuits," in *Proc. ASME Int. Mechanical Engineering Congr. Expo.*, 2001, pp. 1–7.
- [10] R. S. Prasher, "Surface chemistry and characteristics based model for the thermal contact resistance of fluidic interstitial thermal interface materials," *J. Heat Transfer*, vol. 123, pp. 969–975, 2001.
- [11] B. B. Mikic, "Thermal contact conductance: Theoretical considerations," *Int. J. Heat Mass Transfer*, vol. 17, pp. 205–214, 1974.
- [12] V. W. Antonetti, T. D. Whittle, and R. E. Simons, "An approximate thermal contact conductance correlation," *Exper./Numer. Heat Transfer Combust. Phase Change*, vol. 170, pp. 35–42, 1991.
- [13] R. Hill, private communication, 2001.
- [14] *ABAQUS Theory Manual*, Hibbit, Karlsson, and Sorenson, Inc., Pawtucket, RI, 1998.
- [15] V. Tvergaard, "Analysis of tensile properties for a whisker-reinforced metal-matrix composite," *Acta Metall. Mater.*, vol. 38, pp. 185–194, 1990.
- [16] H. J. Bohm, F. G. Rammerstorfer, and E. Weissenbek, "Some simple models for micromechanical investigations of fiber arrangement effects in MMCs," *Computat. Mater. Sci.*, vol. 1, pp. 177–194, 1993.
- [17] V. Singhal, S. V. Garimella, and T. Siegmund, "Determination of optimal filler volume fraction for thermal interface materials in electronics cooling applications," in *Proc. Int. Heat Transfer Conf.*, vol. 3, Grenoble, France, 2002, pp. 9–14.



Vishal Singhal received the B.Tech. degree in energy engineering from the Indian Institute of Technology, Kharagpur, in 2000 and the M.S. degree in mechanical engineering from the Purdue University, West Lafayette, IN, in 2001 where he is currently pursuing the Ph.D. degree in the School of Mechanical Engineering.

His research is focused on micropumping techniques for integrated microchannel cooling systems.



Thomas Siegmund received the Ph.D. degree from the University of Leoben, Austria, in 1995.

He held two positions as Research Associate, at Brown University, Providence, RI, from 1995 to 1996, and at the GKSS Research Center, Geesthacht, Germany, from 1996 to 1999. He is currently an Assistant Professor in the School of Mechanical Engineering, Purdue University, West Lafayette, IN. He has authored 34 articles in referred scientific journals. His research work is in the area of micromechanics of materials with specific focus on

composite materials, mechanics of failure, and time dependent materials.



Suresh V. Garimella received the M.S. degree in mechanical engineering from The Ohio State University, Columbus and the Ph.D. degree in mechanical engineering from the University of California, Berkeley, in 1989.

He is a Professor in the School of Mechanical Engineering, Purdue University, West Lafayette, IN, and the Director of the NSF Cooling Technologies Research Center (CTRC) (an NSF Industry/University Cooperative Research Center). He also directs the Electronics Cooling Laboratory and the Solidification Heat Transfer Laboratory. From 1990 to August 1999, he held the Cray-Research Named Professorship at the University of Wisconsin, Milwaukee. He has published over 150 papers in archival journals and in conference proceedings, and has also contributed to, and edited, several books. He has served as Editor of *Heat Transfer-Recent Contents* and on the Editorial Board of *Experimental Thermal and Fluid Science*. His research interests include high-performance compact cooling technologies, electronics packaging and cooling, micro- and nano-scale thermal phenomena, and electronic and composite materials processing.

Dr. Garimella received the Graduate School/UWM Foundation Research Award in recognition of Outstanding Research and Creative Activity, in 1995, the UWM Distinguished Teaching Award in recognition of Demonstrated Dedication to Excellence in Undergraduate Instruction, in 1997, and the Society of Automotive Engineers' Ralph R. Teetor Educational Award, in 1992. He is a Fellow of the ASME and a member of the K-16 (Heat Transfer in Electronic Equipment) Committee of the Heat Transfer Division of the ASME.